Synergy between thermal spike and exciton decay mechanisms for ion damage and amorphization by electronic excitation

F. Agulló-López,[1,2,*] A. Mendez,[1,2] G. García,[1,†] J. Olivares,[3,1] and J. M. Cabrera[2]
[1]*Centro de Microanálisis de Materiales (CMAM), Universidad Autónoma de Madrid, Cantoblanco, 28049 Madrid, Spain*
[2]*Departamento de Física de Materiales, Universidad Autónoma de Madrid, Cantoblanco, 28049 Madrid, Spain*
[3]*Instituto de Óptica "Daza de Valdés," CSIC, 28004 Madrid, Spain*
(Received 9 August 2006; published 14 November 2006)

A theoretical model is proposed to account for the damage and amorphization induced in $LiNbO_3$ by ion bombardment in the electronic energy-loss regime. It relies on the synergy between the thermal spike generated by electron-phonon interaction and the nonradiative decay of localized (self-trapped) excitons. Calculations have been carried out to describe the effect of single impact as well as multiple impact (high fluence) irradiations. In the first case, the defect concentration profile and the radius of the amorphous tracks have been theoretically predicted and they are in good accordance with those experimentally determined. For high fluence irradiations ($\geq 10^{13}$ cm^{-2}) the model predicts the formation of homogeneous amorphous surface layers whose thickness increases with fluence. The propagation of the crystalline-amorphous boundary has been determined as a function of irradiation fluence. Theoretical predictions are also in good agreement with experimental data on Si-irradiated (7.5 and 5 MeV) $LiNbO_3$ outside the region of nuclear collision damage.

DOI: 10.1103/PhysRevB.74.174109 PACS number(s): 61.80.Az, 34.50.Fa, 61.80.Jh, 79.20.Rf

I. INTRODUCTION

Ion irradiation and implantation are very useful methods to modify dielectric and semiconductor materials and produce devices.[1] They mostly use energies below or around 1 MeV and relatively light atoms so that the damage processes are dominated by nuclear collisions. More recently it has been shown that medium-mass atoms having energies above ~0.1 MeV/amu (swift ions) produce strong damage, amorphization, and phase transformations along their trajectories in many insulators and semiconductors. The effect, caused by electronic excitation mechanisms, is essentially determined by the *electronic stopping power* S_e and appears remarkably different from the damage created through nuclear collisions.[1] Most meaningful experiments performed so far have involved single-impact irradiation, Fig. 1(a). It has been shown[2–6] that when S_e is above a certain *intrinsic threshold* S_{th} a latent (amorphous) track of nanometer diameter is generated along each ion trajectory (*thresholding* behavior) following ion impact. The diameter has been shown to increase monotonically with stopping power.

On the other hand, a variety of recent experiments[7–11] performed on $LiNbO_3$ have shown that for stopping powers above the single-impact threshold and high enough fluences ($\phi \geq 10^{13}$ cm^{-2}), where individual tracks overlap, a full homogeneous amorphous layer is generated, Fig. 1(b). Moreover, the crystal-amorphous boundary propagates deeper into the crystal with irradiation and so the thickness of the amorphous layer increases with ϕ. These data reveal that the ion-beam damage caused by electronic excitation is permanent and cumulative. As a consequence the *effective threshold*, $S_{th}^{eff}(\phi)$, for amorphization depends on fluence ϕ and it is reduced by the defects created by a previous irradiation [obviously, $S_{th}^{eff}(0)=S_{th}$]. In fact, the position of the boundary after fluence ϕ determines the effective threshold by comparison to the stopping power curve as a function of depth. The behavior has been experimentally observed under a variety of irradiation conditions, O (5 MeV and 11 MeV), F (5 MeV), Cl (30 MeV and 45 MeV), and Si (5 MeV, 7.5 MeV, and 30 MeV). It is exemplified for the data obtained[8–10] with Si ions having 5 MeV and 7.5 MeV that are schematically illustrated in Fig. 2. Figure 2(a) shows the stopping power curve for Si ions (7.5 MeV at the surface) as a function of depth z. For comparison purposes the depth reached by the crystal-amorphous boundary is represented in Fig. 2(b). One sees that at larger depths where stopping power is lower the fluences required to reach amorphization are correspondingly larger. Finally, Fig. 3 plots the dependence of effective threshold on fluence derived from Fig. 2. The relevant feature is that the data points corresponding to both, Si at 5 MeV and Si at 7.5 MeV, fit into the same curve, showing that the damage process is essentially dependent on the deposited excitation energy and so on stopping power.

One should note that the problem of material modification and damage induced by electronic excitation is of maximum relevance for other fields of radiation-matter interaction in inorganic, organic, and even biological materials. One may stand out: femtosecond laser-induced damage, ablation and sputtering induced by femtosecond laser pulses,[12–18] amorphization and recrystallization by low-energy electron irradiation,[19,20] and other related physicochemical effects as

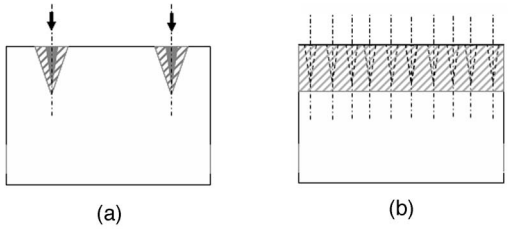

FIG. 1. Schematic illustration of the effect of irradiation in the electronic excitation regime above the electronic stopping threshold: (a) single impact (amorphous track core plus defective halo); (b) high fluence (homogeneous amorphous layer).

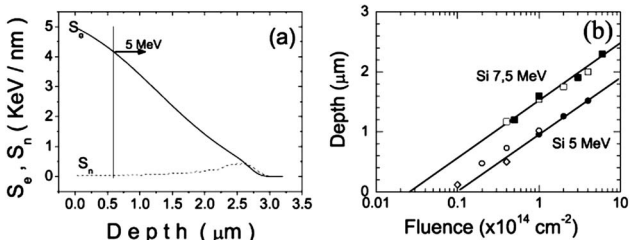

FIG. 2. (a) Electronic S_e and nuclear S_n stopping powers as a function of depth in $LiNbO_3$ for Si having 7.5 MeV at the surface. (b) Displacement of the amorphous crystalline boundary with irradiation fluence.

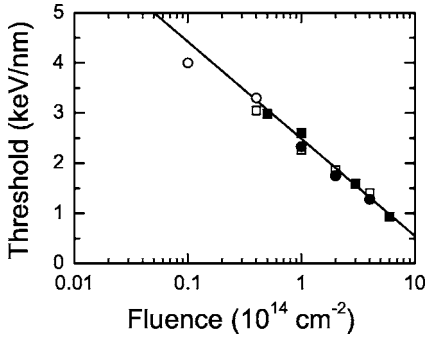

FIG. 3. Effective threshold to start amorphization versus irradiation fluence inferred from the data in Fig. 2.

radiation-enhanced diffusion and clustering,[21,22] and radiation-induced electrical degradation.[23] From the technological side electronic damage should have a relevant impact on the behavior of dielectric (window) materials in fusion reactor technologies.[22,23] The key physical question is how the energy stored after massive electronic excitation is transferred to the lattice and causes bond breaking and point-defect formation.

Unfortunately, at variance with the damage caused by nuclear collisions, the disorder produced in the electronic regime is poorly known and constitutes a matter of active controversy. Several theoretical models have been applied to the description of the amorphization caused by electronic excitation, such as thermal spike,[24,25] Coulomb explosion,[26] or molecular dynamics (MD) calculations.[27,28] So far, in spite of its simplicity, the thermal spike model has been mostly used to account for some relevant features of the amorphization process by single-ion impact. In this model the crystal does not develop any disorder (point defects) and keeps structurally unmodified unless the stopping power reaches a certain threshold value characteristic of the crystal. At this point the lattice melts and after rapid cooling becomes amorphous. The model has been able to explain in a reasonable way the dependence of the amorphous track diameter on electronic stopping power. However, this theoretical approach presents several flaws. First, the scheme is *binary* i.e., the regions of the crystal should only show two states, either fully crystalline or amorphous. On the contrary, there is extensive evidence that the crystal becomes strongly damaged even for irradiations below threshold.[29–31] Moreover, the recent experiments performed in the high fluence regime have revealed an additional new feature of the ion-beam induced damage, namely its cumulative character. In other words, the damage produced by a certain fluence adds to that one generated by a previous irradiation. In order to deal with this information the thermal spike model has been recently extended to deal with the preamorphization stage.[11,32] It is proposed that, below as well as above the electronic stopping threshold, one has to take into account the defects that are thermally generated. The generation rate involves an Arrhenius-type law whose exponent contains the intrinsic formation enthalpy of some suitable point defect. This dependence provides the *superlinearity* required by thresholding. The predictions of the model are in reasonable accordance with the experiment.[11,32] However, some difficulties of such model are connected with the need for thermal equilibrium and with the cumulative character of defect generation. Therefore, other alternative theoretical schemes should be explored.

In this paper we develop an alternative model based on the nonradiative decay of excitons that are self-trapped in the lattice. The model here is applied to $LiNbO_3$ where significant data have been gathered both in the single- and multiple-track regimes. Moreover, it allows for a comparison to the thermal spike models used so far. The problem takes us back to the early days of photolitic (x-rays and UV) damage of ionic materials such as alkali halides,[33] where it was ascertained that defects were created by nonradiative decay of localized (self-trapped) excitons. This idea was later recovered and discussed, at a qualitative level, as a reasonable mechanism to account for laser, electron, and swift-ion damage[16,34,35] in dielectric materials. The present work puts the model on a quantitative basis using features of the thermal spike model. The new synergic model appears quite promising and yields reasonable agreement with experiment for single impact as well as for high fluence irradiations. It may serve to promote a better understanding of electron excitation damage in dielectric materials.

II. EXCITON-DECAY MODEL OF DAMAGE: GENERAL FORMULATION

It is known[33] that excitons are created by ionizing radiation and become self-trapped in alkali halides, alkaline earth fluorides, and many oxides.[36] In the case of $LiNbO_3$, the information available is more scarce, although it is documented that electrons are self-trapped as polarons[33,37] and that self-trapped excitons are very likely formed during irradiation. In fact, a blue intrinsic luminescence band at ~450 nm has been associated to electron-hole recombination at regular niobate groups.[38,39] As for alkali halides it is proposed here that point defects are created via nonradiative decay of self-trapped excitons. However, there is a substantial difference between the two cases. For alkali halides, experiments mostly used low or moderate energy deposition levels and a *thresholding behavior* was *not observed*. In our ion-beam experiments the occurrence of a well-defined threshold requires that in any suitable model the defect production rate should depend on the deposited energy (and so on S_e) in a strongly *superlinear* way. Therefore, in this paper

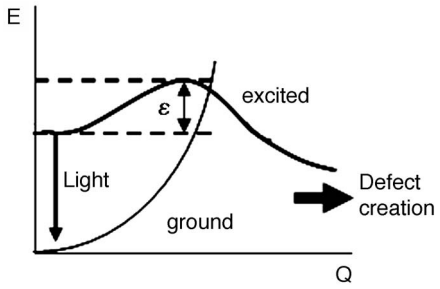

FIG. 4. Schematic level diagram showing the energy E of the ground and excited electronic states of a self-trapped exciton as a function of a configurational coordinate Q. The energy barrier ϵ for nonradiative exciton decay and defect creation has been indicated.

we are going to exploit the possible synergy between such excitonic mechanism and a thermal spike to account for the thresholding behavior and for the main features of the damage and amorphization processes in $LiNbO_3$.

The theoretical scheme we propose is as follows: The first step in swift-ion bombardment is to generate, in about 10^{-16} s, an excited electron cloud along the ion trajectory. The generated electrons very rapidly (in times well below 1 ps) transfer kinetic energy to the lattice, creating phonons (*thermal spike*), and generate new free electrons through atom ionization. After electron thermalization bound electron-hole pairs (excitons) are formed which become homogeneously localized (*self-trapped*) in the crystal lattice. It is estimated that the total number of electron-hole pairs created by S_e is S_e/I, I being an effective ionization energy about 2–3 times the band-gap energy.[34,35] The final step is the exciton decay via either light emission or nonradiative recombination. The nonradiative channel is considered to be the key process giving rise to lattice displacement in a way similar to the case of alkali halides. However, the *synergy* between the *thermal spike* and the *exciton decay* processes is essential to provide the *superlinearity* in the defect generation rate that is experimentally observed. In order to implement such a synergy one assumes for the exciton a schematic energy level diagram as illustrated in Fig. 4. It shows the adiabatic potential energy curves for the ground and excited electronic states as a function of an effective configurational coordinate for the ions. The excited level leads to atom displacement and Frenkel pair formation if the excited electron overcomes a certain energy barrier ϵ. The high temperature reached in the spike provides the needed kinetic energy. The decay of the exciton concentration N_x obeys the rate equation

$$\frac{dN_x}{dt} = -N_x\left\{\nu_0 e^{-\epsilon/kT} + \frac{1}{\tau_R}\right\}, \tag{1}$$

ν_0 being a frequency factor, and τ_R the radiative lifetime. In spite of the scarcity of data, the competition between radiative and nonradiative processes expressed by Eq. (1) is consistent with experimental data[38,39] showing a thermally-activated decrease in the exciton emission band.

The nonradiative decay term in Eq. (1) yields the defect generation rate, providing the required *strong nonlinear dependence of the damage rate on* S_e. The temperature T to include in the exponent of the Arrhenius law is the local temperature in the spike that is a function of time and position. This has to be calculated from S_e following the standard procedures in the thermal spike model (see below). It is clear that defects will be preferentially generated at times and places in the spike where the temperature is high enough. Once the spike has cooled down in times of the order of 10^{-11} s the radiative term having a longer lifetime will dominate and energy will be dissipated through light emission. Integration of that defect production rate over time and over the extension of the spike should yield the total number of defects created by the ion impact. The details are given in the following sections. Our model, finally, assumes that the irradiation triggers a lattice collapse and induces amorphization at a given spot when the defect concentration reaches a critical value n_V^*. The occurrence of an abrupt transition is consistent with the latent track observations as well as with the sharp boundaries separating the crystalline (defective) and amorphous regions when examined by dark-mode[8–10] and micro-Raman[9,10] spectroscopies. In a nonirradiated crystal the amorphization should just occur when the stopping power that determines the energy deposited in the spike equals the threshold level S_{th}. There are, indeed, well documented[40] examples of defect-driven transitions. However, in our case the details and thermodynamics of such transition need to be understood. In particular, the relationship to standard crystal melting should be clarified. Although this point is not critical for our model we think that this collapse should occur close but somewhat below the melting temperature at the spike.

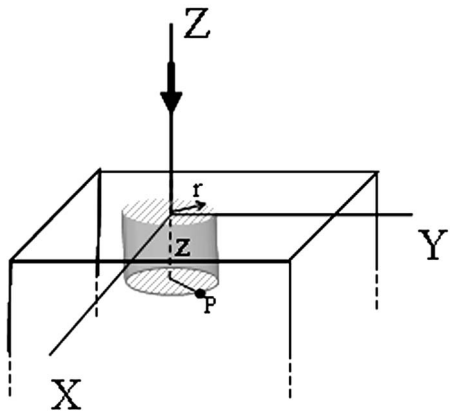

FIG. 5. Geometry for a single-impact irradiation.

III. DAMAGE BY A SINGLE-IMPACT: LATENT TRACK

Let us apply the above model to calculate the defects generated by a single ion impact, Fig. 5. Using cylindrical coordinates (z,r) around the trajectory as Z axis, the integrated number of defects $n_L(z)$ per unit depth (linear defect density) is

$$n_L(z) = \int_0^\infty 2\pi dr n_V(r,z)$$

$$= \int_0^\infty 2\pi r dr \int_0^\infty dt \nu_0 e^{-\epsilon/kT(r,z,t)} N_x(z,r,t), \tag{2}$$

where $n_V(r,z)$ is the local defect concentration at (r,z) and

$N_x(z,r,t)$ and $T(z,r,t)$, respectively, stand for the spatial and temporal profiles of the local concentration of created excitons and track temperature. The initial instant $t=0$ is taken once both the spike and exciton profiles have been formed at the end of the heating process. For $T(r,t)$ we assume that it follows, during cooling, a Gaussian profile given by[41]

$$T(z,r,t) = \Delta T(z,0,t)\exp\{-r^2/a^2(t)\} + T_S, \tag{3}$$

where T_S is the substrate temperature and

$$\Delta T(z,0,t) = \frac{a_0^2 \Delta T(z,0,0)}{a^2(t)}, \tag{4a}$$

is the temperature increase caused by the ion impact. The time evolution of the profile width

$$a^2(t) = a_0^2 + \frac{4K}{\rho C}t \tag{4b}$$

is readily obtained from solving the heat conduction equation. K, C, and ρ, respectively, stand for the thermal conductivity, specific heat and density of the material. On the other hand, the initial temperature rise $\Delta T(z,0,0)$ at the spike axis is related to the electronic stopping power $S_e(z)$ by[41]

$$\Delta T(z,0,0) = \frac{g S_e(z)}{\pi a_0^2 \rho C}, \tag{5}$$

where g is an electron-phonon coupling parameter that measures the efficiency of energy transfer from the electronic system to the lattice. As in the thermal spike model,[41] a value of g is taken as to reach the melting temperature for $S_e = S_{th}$.

As to the exciton distribution, it is assumed to be stationary (diffusion is ignored) and that follows the irradiation-induced temperature profile at the start of the cooling process ($t=0$), i.e.,

$$N_x(z,r,0) = \frac{1}{\pi a_0^2}\frac{S_e(z)}{I} e^{-r^2/a_0^2}. \tag{6}$$

This specific assumption does not essentially affect the physics of the process and it has been shown (see below) that it does not substantially modify the conclusions of this work. From the temperature evolution (3) of the spike, the exciton decay kinetics $N_x(z,r,t)$ can be easily obtained by solving Eq. (1) with the initial Gaussian profile $N_x(z,r,0)$ and the normalization condition (6). Then, Eq. (2) is used to calculate the profile of point defect concentration in the track.

Moreover, we should use the fact that when the electronic stopping power reaches the threshold level S_{th}, the defect concentration has reached the critical level $n_V^* = n_V(S_{th})$ to cause amorphization. For the moment, the specific value of this concentration is not necessary (it will be calculated below) and it can be taken as a reference to normalize all concentrations. Using this method, the normalized defect concentration profiles, $n(r,S_e) = n_V(r,S_e)/n_V^*$, for three ratios of the electronic stopping power to the intrinsic threshold value, $S_e/S_{th} = 0.5$, 1, 1.5, have been determined and are illustrated in Fig. 6. The calculation of n_V requires numerical integration of Eq. (2) after introducing the exciton kinetics and a suitable selection of the relevant parameters: ν_0, S_{th}, I, a_0, and ϵ. Three out of these parameters are approximately known from independent experiments[9,25,33] ($a_0 \cong 4.5$ nm and $S_{th} \approx 3-8$ keV/nm) or can be estimated ($\nu_0 \approx 10^{11}-10^{13}$ s^{-1}, $I \approx 8-12$ eV), so that ϵ remains the only free (adjustable) parameter. A suitable option inferred from all results obtained in this paper is $\epsilon = 0.34$ eV. The results are *independent* of the radiative lifetime τ_R as long as $\tau_R \leq 10^{-5}$ s, to guarantee that the radiative channel is dominant after cooling. Although reliable values are not available this condition does not appear unrealistic.

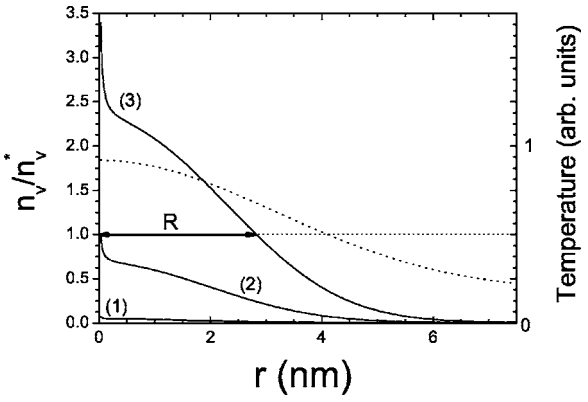

FIG. 6. Defect concentration profiles (continuous lines) for three different values of the ratio S_e/S_{th}: (1) $S_e/S_{th}=0.5$; (2) $S_e/S_{th}=1$; and (3) $S_e/S_{th}=1.5$. The temperature profile in arbitrary units is also indicated by the dashed lines. Parameter values are: $a_0 \cong 4.5$ nm, $I=10$ eV, $S_{th}=5$ keV/nm, and $\nu_0 = 10^{12}$ s^{-1}.

The temperature profile at $t=0$ (and so the exciton profile) is also shown for comparison in Fig. 6. For stopping powers above threshold the critical concentration is reached within a certain radius around the trajectory axis and constitute the amorphous core of the track. At larger radius, defects are also generated and form what is called the halo of the track. Below threshold only defects (halo) are formed. It has been checked that the model predictions are robust in the sense that the detailed exciton profile is not critical. In fact, assumed profiles whose width differs by a factor 2 from that corresponding to the temperature only produces minor changes in the defect concentrations.

The dependence of the core radius of the track on stopping power is plotted in Fig. 7. The theoretical predictions are compared with experimental results[25] obtained under different irradiation conditions. The parameters have been chosen as for Fig. 6, except for S_{th} that has been varied from 3 keV/nm to 8 keV/nm to cover the region adequate to the experimental conditions. The agreement is qualitatively reasonable although theoretical values appear somewhat higher than the experimental ones.

IV. DAMAGE AND AMORPHIZATION UNDER A HIGH-FLUENCE IRRADIATION

Let us now describe the process of damage and amorphization under a high enough fluence ($\phi \geq 10^{13}$ cm^{-2}) so that tracks overlap and an average description of the disorder is adequate. This situation also allows for a direct compari-

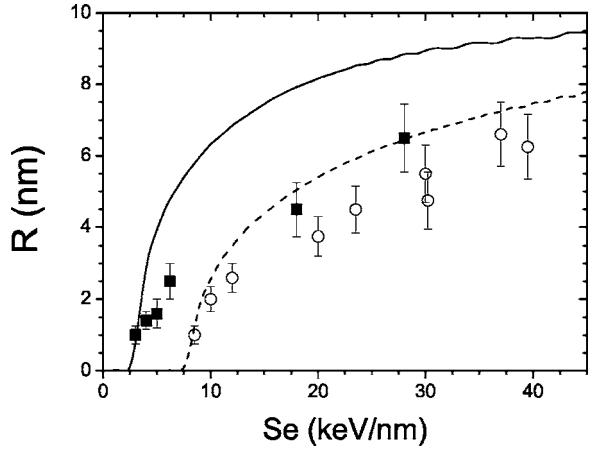

FIG. 7. Dependence of the radius of the track core on stopping power. Experimental data (Ref. 25) are included. The two theoretical curves correspond to $S_{th}=3$ keV/nm (continuous line) and $S_{th}=8$ keV/nm (dashed line).

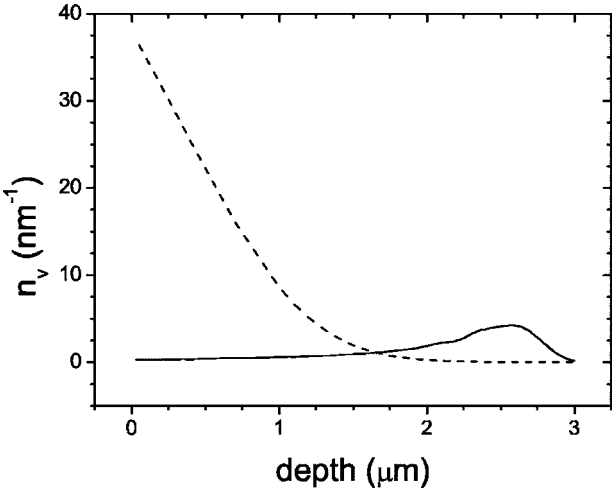

FIG. 9. Comparison between the defects generated by electronic excitation (dashed line) and nuclear collisions (continuous line). Curves correspond to silicon irradiations at 7.5 MeV.

son to experiments[8,9] yielding the position of the crystalline-amorphous boundary during Si irradiations at 5 MeV and 7.5 MeV. The average defect concentration generated in a layer at depth z by an ion fluence ϕ is $N_D(z)=\phi n_L(z)$. In order to induce amorphization that average concentration must reach the critical level causing lattice collapse through the defect-driven transition. It should correspond to the value $n_V(0,z)$ reached at the track center when $S_e=S_{th}$. Then, the position of the amorphous-crystalline boundary obeys the implicit equation

$$N_D[S_e(z_B)] = \phi\, n_L(z_B) = n_V(0,z_B) \tag{7}$$

that yields the boundary depth z_B after a fluence ϕ. The calculation of n_V requires numerical integration of Eq. (2) after introducing the exciton kinetics and a suitable selection of the relevant parameters: ν_0, S_{th}, I, a_0, and ϵ.

For Si irradiations the measured threshold stopping power[9,11] is approximately $S_{th}=5$ keV/nm. Therefore, Fig. 8 shows the results of the calculations corresponding to $\epsilon=0.34$ eV, $\nu_0=10^{12}$ s^{-1}, $I=10$ eV, $a_0=4.5$ nm, and $S_{th}=5$ keV/nm together with the experimental data points,[9,11] for Si irradiations at 5 MeV and 7.5 MeV. For clarity, the low [Fig. 8(a)] and high [Fig. 8(b)] fluence regions have

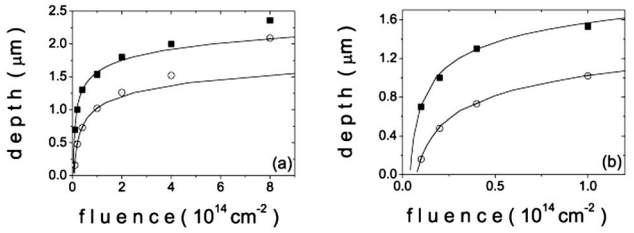

FIG. 8. Experimental data points for the crystalline-amorphous boundary depth as a function of fluence for Si irradiations at 7.5 MeV (solid squares) and 5 MeV (open circles). The simulated curves obtained by solving implicit Eq. (7) are indicated as continuous lines ($\epsilon=0.34$ eV). The high- and low-fluence regions are, respectively, plotted in Figs. 3(a) and 3(b).

been independently plotted. In the two cases the measured trend is well obeyed and even a good quantitative agreement is obtained, particularly for low or moderate fluences (see below). The boundary propagates at a decreasing rate until it approaches a quasi-steady location (saturation stage). Note from Fig. 8(b) that for 5 MeV an initial (*incubation*) fluence of $\approx 10^{13}$ cm^{-2} is required to start the amorphous layer from the surface since $S_e(z=0)=4.1$ keV/nm$<S_{th}$. On the other hand, no prior fluence is necessary for 7.5 MeV where $S_e(z=0)\approx 5$ keV/nm. One should remark that the model is quite robust in the sense that the main physical features and an approximate fitting to experiment is maintained within a reasonable range of values for ν_0 and ϵ. It is also worth noting that one can now calculate the critical concentration n_V^* to start lattice amorphization. It becomes $n_V^*=1.5$ nm^{-3}, which amounts to $\approx 7\%$ of the niobium concentration in the $LiNbO_3$ lattice. Finally, the experimental data in Fig. 8 indicate that for large depths [near the peak of the $S_n(z)$ curve] the boundary propagates deeper in the crystal than predicted by the excitonic mechanism, suggesting additional damage caused by nuclear collisions. This view is supported by calculations that compare the number of defects created by the electronic mechanism, Eq. (2), and by nuclear collisions (using the SRIM 2003 code[42]). The results of the calculations are shown in Fig. 9. The data for other ions (O at 5 MeV, and 11 MeV, and F at 5 MeV) can also be reasonably fitted by the model if one slightly changes the threshold value. These changes are expected from the known effect of ion velocity on ion-beam damage as measured[25] in recent single impact experiments on $LiNbO_3$.

V. SUMMARY AND CONCLUSIONS

In summary, a theoretical model based on the nonradiative decay of excitons has been proposed which reasonably accounts for the damage and amorphization produced by swift ions in the single- and multiple-impact (high fluence) regimes in $LiNbO_3$. It exploits the synergy between the ther-

mal spike generated by the ion impact and the exciton decay kinetics to provide the required superlinear dependence of the damage on the electronic stopping power. The low fluence region where the statistics of ion impacts is relevant has not been investigated. Further extensions of the model should include the effect of such statistical fluctuations, e.g., by using a Monte Carlo strategy.[35] It is expected that the proposed model could be extended to describe amorphization effects in other materials, mainly oxides. It might also describe some of the effects (e.g., incubation stage and crater growth) observed in experiments using femtosecond laser pulses.

*Corresponding author. Email address: fal@uam.es
†Present address: CELLS, 08193 Bellaterra, Barcelona, Spain.

[1] P. D. Townsend, P. J. Chandler, and L. Zhang, *Optical Effects of Ion Implantation* (Cambridge University Press, Cambridge, 1994).
[2] R. Spohr, in *Ion Tracks and Microtechnology: Basic Principles and Applications*, edited by K. Bethge (Vieweg, Braunchsweig, 1990).
[3] B. Canut, A. Benyagoub, G. Marest, A. Meftah, N. Moncoffre, S. M. M. Ramos, F. Studer, P. Thevenard, and M. Toulemonde, Phys. Rev. B **51**, 12194 (1995).
[4] A. Benyagoub, F. Levesque, F. Couvreur, C. Gibert-Mougel, C. Dufour, and E. Paumier, Appl. Phys. Lett. **77**, 3197 (2000).
[5] P. I. Gaiduk, A. Nylansted-Larsen, J. Lundsgaard-Hansen, C. Trautmann, and M. Toulemonde, Appl. Phys. Lett. **83**, 1746 (2003).
[6] G. Szenes, Z. E. Horvath, B. Pecz, F. Paszti, and L. Toth, Phys. Rev. B **65**, 045206 (2002).
[7] G. G. Bentini, M. Bianconi, L. Correra, M. Chiarini, P. Mazzoldi, C. Sada, N. Argiolas, M. Bazzan, and R. Guzzi, J. Appl. Phys. **96**, 242 (2004).
[8] J. Olivares, G. Garcia, F. Agulló-López, F. Agulló-Rueda, J. C. Soares, and A. Kling, Nucl. Instrum. Methods Phys. Res. B **242**, 534 (2005).
[9] J. Olivares, G. García, F. Agulló-López, F. Agulló-Rueda, A. Kling, and J. C. Soares, Appl. Phys. A **81**, 1465 (2005).
[10] J. Olivares, G. García, A. García-Navarro, F. Agulló-López, O. Caballero, and A. García-Cabañes, Appl. Phys. Lett. **86**, 183501 (2005).
[11] Agulló-López, G. García, and J. Olivares, J. Appl. Phys. **97**, 093514 (2005).
[12] R. Kelly and A. Miotello, Mater. Sci. Forum **301**, 145 (1999).
[13] D. Ashkenasi, M. Lorenz, R. Stoian, and A. Rosenfeld, Appl. Surf. Sci. **150**, 101 (1999).
[14] H. B. Sun, Y. Xu, S. Juodkazis, K. Sun, M. Watanabe, S. Matsuo, H. Misawa, and J. Nishii, Opt. Lett. **26**, 325 (2001).
[15] E. A. Stach, V. Radmilovic, D. Deshpande, A. Malshe, D. Alexander, and D. Doerr, Appl. Phys. Lett. **83**, 4420 (2003).
[16] S. S. Mao, F. Queré, S. Guizard, X. Mao, R. E. Russo, G. Petite, and P. Martin, Appl. Phys. A **79**, 1695 (2004).
[17] J. Bonse, S. M. Wiggins, and J. Solis, Appl. Phys. A **80**, 243 (2005).
[18] D. Deshpande, A. P. Malshe, E. A. Stach, V. Radmilovic, D. Alexander, D. Doerr, and D. Hirt, J. Appl. Phys. **97**, 074316 (2005).
[19] M. W. Bench, I. M. Robertson, M. A. Kirk, and I. Jencik, J. Appl. Phys. **87**, 49 (2000).
[20] J. Frantz, J. Tarus, K. Nordlund, and J. Keinonen, Phys. Rev. B **64**, 125313 (2001).
[21] S. Clement and E. R. Hodgson, Phys. Rev. B **36**, 3359 (1987).
[22] A. Moroño and E. R. Hodgson, J. Nucl. Mater. **250**, 156 (1997).
[23] E. R. Hodgson and A. Moroño, J. Nucl. Mater. **283**, 880 (2000).
[24] M. Toulemonde, Ch. Dufour, A. Meftah, and E. Paumier, Nucl. Instrum. Methods Phys. Res. B **166**, 903 (2000).
[25] A. Meftah, J. M. Constantini, N. Khalfaoui, S. Boudjadar, J. P. Stoquert, F. Studer, and M. Toulemonde, Nucl. Instrum. Methods Phys. Res. B **237**, 563 (2005).
[26] E. M. Bringa and R. E. Johnson, Phys. Rev. Lett. **88**, 165501-1 (2002).
[27] E. M. Bringa, R. E. Johnson, and M. Jakas, Phys. Rev. B **60**, 15107 (1999).
[28] M. M. Jakas, E. M. Bringa, and R. E. Johnson, Phys. Rev. B **65**, 165425 (2002).
[29] J. Vetter *et al.*, Nucl. Instrum. Methods Phys. Res. B **91**, 129 (1994).
[30] G. G. Bentini, M. Bianconi, M. Chiarini, L. Correra, C. Sada, P. Mazzoldi, N. Argiolas, M. Bazzan, and R. Guzzi, J. Appl. Phys. **92**, 6477 (2002).
[31] J. Olivares, A. García-Navarro, G. García, A. Méndez, and F. Agulló-López, Appl. Phys. Lett. **89**, 071923 (2006).
[32] G. García, F. Agulló-López, J. Olivares, and A. García-Navarro, J. Appl. Phys. **99**, 1 (2006).
[33] F. Agulló-Lopez, R. C. Catlow, and P. D. Townsend, *Point Defects in Materials* (Academic Press, London, 1984).
[34] N. Itoh and A. M. Stoneham, Nucl. Instrum. Methods Phys. Res. B **146**, 362 (1998).
[35] N. Itoh, Nucl. Instrum. Methods Phys. Res. B **135**, 175 (1998).
[36] V. Murk, Mater. Sci. Forum **239-241**, 537 (1997).
[37] *Insulating Materials for Optoelectronics: New Developments*, edited by F. Agulló-López (World Scientific, Singapore, 1995).
[38] P. W. Haycock and P. D. Townsend, J. Phys. C **20**, 319 (1987).
[39] *Properties of Lithium Niobate*, edited by K. K. Wong (EMIS Datareview Series, INSPEC, Exeter, 2002).
[40] H. J. Fecht, Nature (London) **356**, 133 (1992).
[41] G. Szenes, Phys. Rev. B **51**, 8026 (1995).
[42] *The Stopping and Ranges of Ions in Solids*, edited by J. F. Ziegler, J. P. Biersack, and U. Littmark (Pergamon, New York, 1985); see also the SRIM web page http://www.srim.org